




Rates of pyruvate carboxylase, glutamate and GABA neurotransmitter cycling, and glucose oxidation in multiple brain regions of the awake rat using a combination of [2-¹³C]/[1-¹³C]glucose infusion and ¹H-[¹³C]NMR *ex vivo*

Laura M McNair¹ , Graeme F Mason^{2,3,4},
Golam MI Chowdhury³, Lihong Jiang², Xiaoxian Ma²,
Douglas L Rothman^{2,4}, Helle S Waagepetersen¹ and
Kevin L Behar³

Abstract

Anaplerosis occurs predominately in astroglia through the action of pyruvate carboxylase (PC). The rate of PC (V_{pc}) has been reported for cerebral cortex (or whole brain) of awake humans and anesthetized rodents, but regional brain rates remain largely unknown and, hence, were subjected to investigation in the current study. Awake male rats were infused with either [2-¹³C]glucose or [1-¹³C]glucose ($n = 27/30$) for 8, 15, 30, 60 or 120 min, followed by rapid euthanasia with focused-beam microwave irradiation to the brain. Blood plasma and extracts of cerebellum, hippocampus, striatum, and cerebral cortex were analyzed by ¹H-[¹³C]-NMR to establish ¹³C-enrichment time courses for glutamate-C4,C3,C2, glutamine-C4,C3, GABA-C2,C3,C4 and aspartate-C2,C3. Metabolic rates were determined by fitting a three-compartment metabolic model (glutamatergic and GABAergic neurons and astroglia) to the eighteen time courses. V_{pc} varied by 44% across brain regions, being lowest in the cerebellum ($0.087 \pm 0.004 \mu\text{mol/g/min}$) and highest in striatum (0.125 ± 0.009) with intermediate values in cerebral cortex (0.106 ± 0.005) and hippocampus (0.114 ± 0.005). V_{pc} constituted 13–19% of the oxidative glucose consumption rate. Combination of cerebral cortical data with literature values revealed a positive correlation between V_{pc} and the rates of glutamate/glutamine-cycling and oxidative glucose consumption, respectively, consistent with earlier observations.

Keywords

Anaplerosis, cerebellum, cerebral cortex, hippocampus, striatum

Received 2 June 2021; Revised 1 November 2021; Accepted 30 November 2021

Introduction

The majority of excitatory and inhibitory neurotransmission in brain employs neurotransmitter glutamate and γ -aminobutyric acid (GABA), respectively, and availability of these transmitters is crucial for brain function. Molecules of neurotransmitter glutamate and GABA and their glutamine precursors are lost by oxidation, diffusion through the extracellular space to blood or employed to remove excess ammonia.^{1–4} Any loss requires a balanced *de novo* synthesis. In brain *de*

¹Department of Drug Design and Pharmacology, Faculty of Health and Medical Sciences, University of Copenhagen, Copenhagen, Denmark
²Department of Radiology and Biomedical Imaging, Magnetic Resonance Research Center, Yale University School of Medicine, New Haven, Connecticut, USA
³Department of Psychiatry, Yale University School of Medicine, New Haven, Connecticut, USA
⁴Department of Biomedical Engineering, Yale University, New Haven, Connecticut, USA

Corresponding authors:

Laura M McNair, Jagtvej 160, 2100 Copenhagen Ø, Denmark.
Email: laura.mcnaair@sund.ku.dk

Kevin L Behar, Yale University, MRRC TAC N151, 300 Cedar St, PO Box 208043, New Haven, Connecticut 06520, USA.
Email: kevin.behar@yale.edu

novo synthesis from glucose occurs *via* pyruvate carboxylase (PC), a mitochondrial enzyme confined to astroglia.^{5–10} PC catalyzes the carboxylation of pyruvate, the end-product of glycolysis, to form and increase the pool of the Tricarboxylic Acid (TCA) cycle intermediate oxaloacetate (OAA). The process of increasing the TCA cycle carbon pool is termed anaplerosis and forms the basis for *de novo* synthesis of glutamine, a precursor for neurotransmitter glutamate and GABA.^{11–18}

The quantitative significance of anaplerosis to brain glucose metabolism has been addressed in magnetic resonance spectroscopy studies of rodents *in vitro* and *in vivo*,^{19–30} as well as in humans,^{31–33} but only for whole brain (excluding cerebellum) or cerebral cortex. Some studies indicate that metabolic flux through PC (V_{pc}), like glucose oxidation and neurotransmitter cycling, varies with level of brain activity,^{27,30} i.e. higher in the awake animal and lower under anesthesia, suggesting a more central role for PC in energy metabolism. Other studies show no change in V_{pc} over baseline with stimulation,^{25,34,35} hence a correlation between V_{pc} and brain activity may depend on the mechanism underlying the changed brain activity level.

Anaplerosis *via* PC has been measured using different isotopic labels and substrates, including H¹⁴CO₂, [1-¹³C]glucose and [2-¹³C]glucose.^{19,30,33,36,37} While highly specific, the measurement of fixed carbon from H¹⁴CO₂ provides net flux through PC but no information on competing metabolic pathways, like flux through pyruvate dehydrogenase (V_{pdh}). In contrast, labeling brain amino acids from ¹³C-glucose, when coupled with nuclear magnetic resonance (NMR) spectroscopy or mass spectrometry (MS) detection and metabolic modeling, provides quantitative flux estimates of V_{pc}, as well as V_{pdh} and several other fluxes relevant to the energetic status of neural tissue. However, [1-¹³C] and [2-¹³C]glucose assay V_{pc} differently, with differing specificities. Of the two, the assay of V_{pc} using [2-¹³C]glucose possesses the highest specificity and sensitivity, as labeling of the reporter amino acid, glutamine-C2 and -C3, is not confounded by PDH metabolism of [2-¹³C]pyruvate, nor influenced negatively by cycling between OAA and fumarate, as experienced with the [3-¹³C]pyruvate made from [1-¹³C]glucose.

Anaplerosis in terms of CO₂ fixation of pyruvate in brain was first demonstrated in the early 1960's by Berl and co-workers^{38,39} and the enzyme which catalyzed this activity, PC, subsequently described.⁴⁰ For a history of the work leading to the localization of PC in astroglia, see.⁴¹ Early estimates of *in vivo* anaplerosis in whole brain using [2-¹⁴C]pyruvate or its precursor [2-¹⁴C]lactate, suggested that under physiologically normal conditions this pathway constitutes 9–14% of

overall pyruvate metabolism.^{42,43} More recent studies employing [1-¹³C]glucose (and H¹⁴CO₂) or [2-¹³C]glucose and NMR reported values for V_{pc} of 0.17–0.18 μmol/g/min and 0.04–0.09 μmol/g/min for the whole brain or cerebral cortex of the awake and anesthetized rat brain, respectively.^{19,20,25–27,30,36} These rates corresponded to ~10–20% of their respective rates of glucose oxidation, and, hence, are within the range of earlier estimates. However, despite the importance of anaplerosis to neurotransmitter homeostasis and normal brain function, its magnitude and relationship to glucose oxidation and neurotransmitter cycling across brain regions, and activities during wakefulness remains largely unknown. This reflects our current poor understanding of the anabolic and catabolic (i.e., glutamate/GABA oxidation) processes that determine anaplerosis over the lifespan.⁴⁴

In the present study, we determined the rates of anaplerosis (V_{pc}), neurotransmitter cycling and glucose oxidation in neurons and astroglia of four brain regions in awake rats receiving timed infusions of either [1-¹³C] or [2-¹³C]glucose, followed by rapid euthanasia. Tissue extracts of the water-soluble metabolites were prepared and measured using ¹H-[¹³C]NMR. The metabolic fluxes were determined by fitting a three-compartment metabolic model (glutamatergic and GABAergic neurons, and astroglia) simultaneously to the time courses of amino acid ¹³C-enrichments produced during the [1-¹³C] and [2-¹³C]glucose infusions.

Materials and methods

Animal preparation and sample processing

Rat experiments were conducted in accordance with the guideline of the National Institutes of Health Guide for the Care and Use of Laboratory Animals and the AVMA Guidelines for the Euthanasia of Animals (2013 Edition), under protocols approved by the Institutional Animal Care and Use Committee of Yale University. All efforts were made to minimize animal suffering according to the Animal Welfare Act administered by USDA. Furthermore, this manuscript is in compliance with the ARRIVE guidelines for how to report animal experiments.

Male Sprague-Dawley rats (210 ± 11 g, n = 57) were acclimatized at least 1 day (5[4–7] days) following arrival from Harlan Laboratories Ltd. (Indianapolis, IN, USA), then fasted overnight and prepared with tail vein catheters under isoflurane anesthesia. Animals were allowed to recover from anesthesia for at least 30 min prior to infusion with 0.75 M [1-¹³C]glucose or [2-¹³C]glucose (99 atom%, Cambridge Isotope Laboratories, Cambridge, MA, USA) dissolved in saline (0.9% NaCl). The ¹³C-glucose solution was

delivered as a 15 sec bolus followed by an exponentially decreasing rate adjusted every 30 sec for the next 8 min and then kept at a steady rate for the remaining infusion time as described previously.⁴⁵ Following 8, 15, 30, 60 or 120 min infusion (5–7 rats/time point/glucose isotope in order to obtain a reasonable estimation of the true means) rats were quickly sedated (<50 sec) with isoflurane (2–3%) and euthanized by Focused Beam Microwave Irradiation to the head (FBMI; Model TMW 6402C, Muromachi Microwave Fixation System, 1.15–1.35 sec, 4.5 kW), arresting brain metabolism.⁴⁶ The brain was removed and dissected into four regions; cerebellum (CB), hippocampus (HP), striatum (ST) and cerebral cortex (CX). Blood was sampled from the caudal vena cava following FBMI into heparin-treated tubes, centrifuged (2500 rpm, 15 min, 4°C), and the plasma collected. Experiments were terminated and samples and/or data excluded when experimental procedures failed, e.g. faulty catheter or problematic FBMI (four of total 61 animals did not complete experiments), or sample processing (total metabolite concentrations were not determined for some extracts due to unintended lack of internal standard). No randomization protocol was used to assign animals to a specific ¹³C-substrate and infusion length prior to the procedures; however, care was taken in order to interchange between these parameters on and between experimental days. Investigators were not blinded to the experimental treatment (i.e. ¹³C-isotope infused) or the processing and analysis of the data.

Blood plasma and brain samples were frozen in liquid N₂ and stored at –80°C for subsequent analysis. Blood plasma was prepared for NMR analysis by filtering thawed samples (Nanosep, 10kD) at 5000 rpm and diluting (1:4) with 90:10 v/v D₂O:H₂O, 0.25 mM TSP and 2.0 mM formic acid in 50 mM KPO₄ buffer (pH = 7.0). Brain samples (24–312 mg) were prepared for NMR analysis as follows: Frozen brain tissue was weighed, extracted in ice-cold 0.1 M HCl in methanol (1:2 tissue weight/volume) and 800 μL 10 mM KPO₄/90% ethanol solution (first extract) and homogenized using an OMNI Bead Ruptor24 (Omni International, GA, USA) followed by centrifugation at 13,000 rpm (30 min, 4°C). The pellet was re-homogenized using 1 mL of 6.7 mM KPO₄/60% ethanol solution, centrifuged, and supernatants combined. [2-¹³C]Glycine was added in the first extraction step as an internal concentration reference. Sample tubes were cooled on dry ice throughout the extraction procedure. The supernatants were filtered through Chelex-100 resin, lyophilized, and reconstituted in 90:10 v/v D₂O:H₂O, 0.25 mM TSP, 50 mM KPO₄ buffer (pH = 7.0).

Nuclear magnetic resonance analysis of brain extract and blood samples ex vivo

Fully relaxed ¹H-[¹³C]-NMR spectra of plasma and brain extracts were acquired at 11.7 T (¹H resonance frequency of 500.13 MHz) using a Bruker AVANCE spectrometer (Bruker Corp., Billerica, MA, USA). ¹H-[¹³C]-NMR spectra were acquired as two subspectra – one involving broadband ¹³C-inversion pulses applied in alternate scan blocks, whereas ¹³C-decoupling was applied in both. Subtraction of the scans obtained with ¹³C-inversion (¹²C–¹³C) from those without inversion (¹²C+¹³C) gave the difference spectrum (2 × ¹³C), containing only ¹³C-coupled ¹H resonances at twice the true intensity.⁴⁷ The total carbon isotope composition was given by the ¹²C+¹³C subspectrum. The percentage ¹³C-enrichment (PE) was calculated as the ratio, (¹³C/(¹²C+¹³C)) × 100, followed by subtraction of 1.1% to remove ¹³C arising from natural abundance.

Absolute concentrations of metabolites in brain tissue extracts were determined relative to [2-¹³C]glycine, added during tissue extraction as an internal concentration reference. In plasma, formate was added as internal standard during sample preparation. The isotopic ¹³C enrichments of glutamate (Glu) C2, C3, and C4, GABA C2, C3 and C4, glutamine (Gln) C3 and C4, and aspartate (Asp) C2 and C3 were calculated from the ratio of the areas of these resonances in the ¹H-[¹³C]-NMR difference spectrum (2 × ¹³C only) and the non-edited spectrum (¹²C+¹³C).^{48,49} Representative ¹H-[¹³C]-NMR spectra are provided in Figure 1.

¹³C-labeling of plasma glucose (H1α at 5.24 ppm and H2α at 3.24 ppm) were determined using ¹H-NMR without ¹³C-decoupling. The PE of glucose-C1α and glucose-C2α were calculated by dividing the areas of the ¹³C-satellites with the total area (¹²C+¹³C) of their respective resonances. In addition, a portion of the plasma was used to measure the total glucose concentration (Glucose Analyzer GM9D, Analox Instruments Ltd., Stourbridge, UK).

Description of the metabolic model and determination of metabolic rates

Three-compartment metabolic model: The time courses of ¹³C-labeling of glutamate (Glu), glutamine (Gln), GABA and aspartate (Asp), were fitted with a metabolic model consisting of three compartments; astroglia and GABAergic and glutamatergic neurons. In this model [1-¹³C]glucose (Figure 2(a)) enters the brain and is metabolized through glycolysis to C3-labeled pyruvate (Pyr). Mitochondrial metabolism of Pyr-C3 by PDH produces C2-labeled acetyl-CoA, which enters the TCA cycle to form C4-labeled

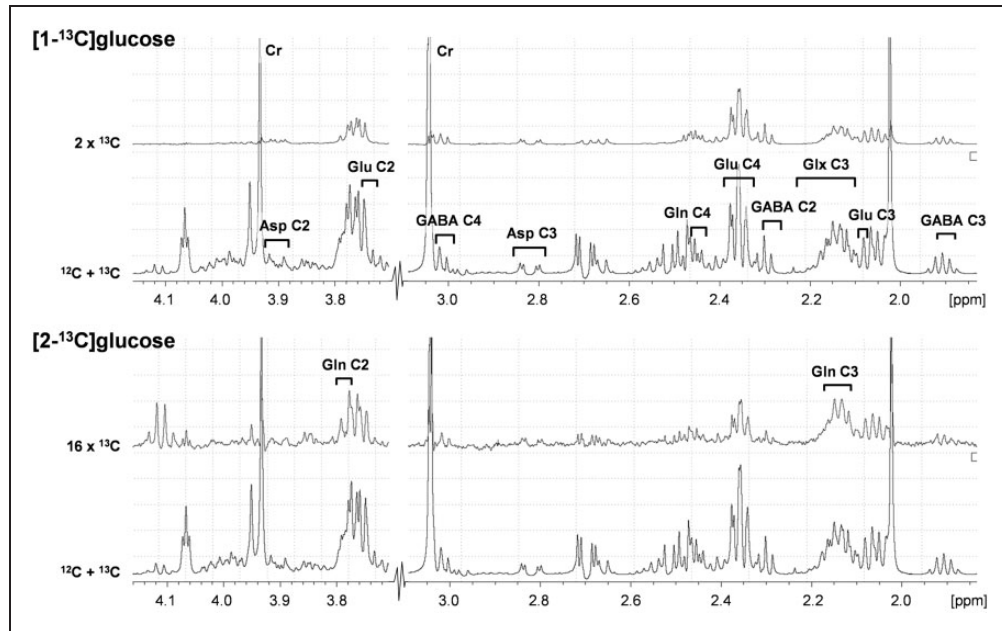


Figure 1. Representative ^1H - ^{13}C NMR spectra from rat cerebral cortex obtained *ex vivo* following infusion with $[1\text{-}^{13}\text{C}]$ glucose (upper two traces) or $[2\text{-}^{13}\text{C}]$ glucose (lower two traces). $^{12}\text{C} + ^{13}\text{C}$ indicates total spectra, and difference spectra have been multiplied to emphasize peaks, hence denoted $2\times^{13}\text{C}$ and $16\times^{13}\text{C}$. Numbers indicate carbon position in glutamate (Glu), glutamine (Gln), glutamate+glutamine (Glx), γ -aminobutyric acid (GABA), and aspartate (Asp).

α -ketoglutarate (αKG). Isotopic exchange between αKG and Glu produces C4-labeled Glu, which is the precursor of C2-labeled GABA. Neurotransmitter Glu-C4 and GABA-C2, generated in the neurons are released from the pre-synaptic terminals during depolarization, and subsequently taken up by surrounding astroglia, in which C4-labeled Gln is generated by glutamine synthetase (GS). Finally, Gln is transferred back to the neuron, thereby completing the Glu/GABA-Gln cycle. Continuation of the carbon through the TCA cycle labels the C2 and C3 of Glu and Gln and the C3 and C4 of GABA.

In astroglia, Pyr labeled at C3 from $[1\text{-}^{13}\text{C}]$ glucose also gives rise to C3-labeled oxaloacetate (OAA) through the astroglia-specific enzyme pyruvate carboxylase (PC). Forward metabolism through the TCA cycle (OAA \rightarrow citrate \rightarrow isocitrate \rightarrow αKG) labels αKG at C2, followed by labeling of Glu and Gln at C2, and GABA at C4. However, back-cycling of the label from OAA to fumarate—a symmetrical molecule—can occur, scrambling (sc) the label to generate C3- and C2-labeled fumarate and OAA, which occurs at the rate V_{sc} . Forward metabolism of C3- and C2-labeled OAA in the TCA cycle leads to C2- and C3-labeled αKG , Glu and Gln, and C4- and C3-labeled GABA. Labeling at the same carbon positions occurs in the second turn of the TCA cycle after the initial entrance of labeling via PDH.

When $[2\text{-}^{13}\text{C}]$ glucose (Figure 2(b)) is metabolized to C2-labeled Pyr through glycolysis, TCA cycle entry via PDH forms C1-labeled acetyl-CoA, labeling αKG at C5, followed by Glu and Gln at C5, and GABA at C1. The second turn of the TCA cycle labels Glu and Gln at C1, and leaves GABA unlabeled.

Thus, because C3 and C2-labeling in Glu and Gln, and C3 and C4-labeling in GABA can only occur *via* PC, $[2\text{-}^{13}\text{C}]$ glucose makes it possible to distinguish PC-derived labeling from labeling *via* PDH.^{23,33,36} In addition, because OAA exchanges with Asp through the action of aspartate aminotransferase, ^{13}C -labeling in OAA is reflected in Asp.

The metabolic model consisted of 104 coupled differential equations and algebraic equations describing mass and isotope balance for C1 and C2-labeled glucose utilization in parallel three-compartment models consisting of glutamatergic and GABAergic neurons, and astroglia.^{50–52} The model was fitted simultaneously to the time course data sets from the $[2\text{-}^{13}\text{C}]$ glucose and $[1\text{-}^{13}\text{C}]$ glucose infusions using CWave 3.5^{53,54} running in MATLAB (The MathWorks, Natick, USA). A copy of CWave can be requested from the software developer and co-author Graeme Mason per mail or e-mail (Graeme.Mason@yale.edu). See supplementary information Table S1 for a mathematical description of the metabolic model and parameters. The driver input consisted of the time courses of blood plasma glucose

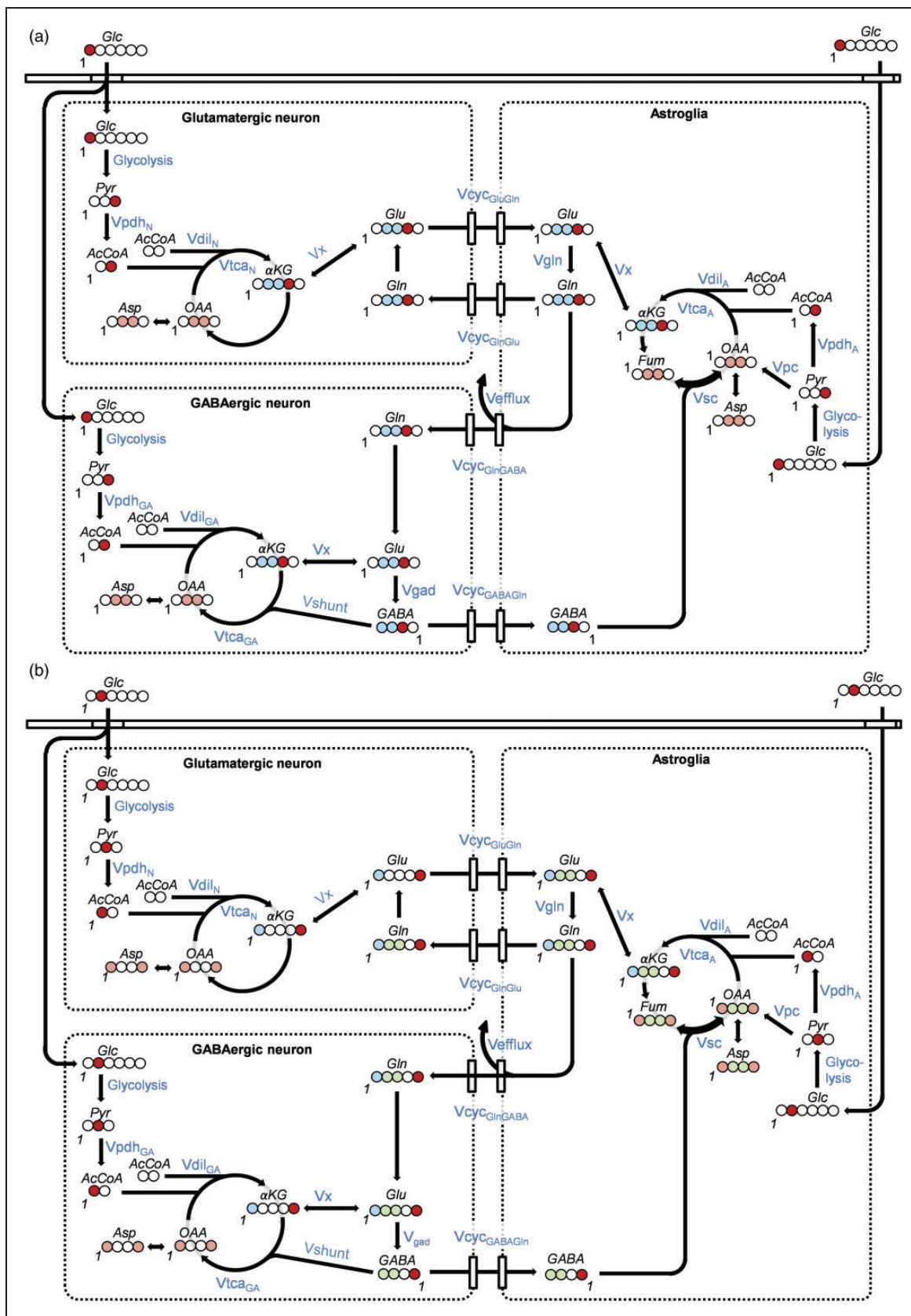


Figure 2. Schematic diagram of the labeling of cerebral metabolites from (a) [1-¹³C]glucose and (b) [2-¹³C]glucose, respectively. Circles represent carbon atoms. Whole filled circles: 100% ¹³C-enrichment at this carbon-position of the molecule; Same color Continued.

concentrations and PE of glucose-C1 and C2. The fitted target data consisted of 18 enrichment time courses, including enrichments for Glu-C2, C3, and C4, GABA-C2, C3, and C4, and Gln-C3 and C4 from infusions with [1-¹³C]glucose or [2-¹³C]glucose, and enrichments for Asp-C2 and C3 from infusions with [1-¹³C]glucose. Fits of the metabolic model to the measured time courses yielded estimates of several key metabolic rates including pyruvate carboxylase (Vpc), TCA cycles (total, Vtca_{Tot}; in glutamatergic and GABAergic neurons, Vtca_N and Vtca_{GA}, respectively; and astroglia, Vtca_A), and Glu/GABA-Gln cycling rates (Vcyc_{GluGln} and Vcyc_{GABAGln}). A complete list of the iterated and calculated rates is provided in supplementary information Table S1.

Two-compartment metabolic model: To assess the potential impact of the three-compartment metabolic model (inclusion of GABA metabolism) on the interpretation of the study findings, the time courses of ¹³C-labeling of glutamate (Glu), glutamine (Gln) and aspartate (Asp) were fitted by a metabolic model consisting of two compartments of glutamatergic neurons and astrocytes.³⁶ This model follows the description of the three-compartment model above but without the GABA pathway and its associated equations.

Statistics

All data were tested for normality using the Shapiro-Wilk test and results are reported as mean ± standard deviations (SD) or median and interquartile range (IQR), [Q3-Q1], as appropriate. Student's t-test and ANOVA were used to compare physiological parameters, and non-parametric statistical analysis, corrected for multiple comparisons, were used for data which passed or did not pass the test for normality, respectively. Test specifications are given along with the statistical output. Statistical analysis were performed using GraphPad Prism software version 9.1.0 for Windows (GraphPad Software, La Jolla, California, USA). Correlation analyses were performed using Spearman's correlation test in Microsoft Excel 2010 or GraphPad Prism.

The uncertainties in the model parameters and their distributions were determined in CWave by Monte-Carlo simulations with 1,000 iterations (three-compartment model) or 500 iterations (two-compartment model).⁵⁴⁻⁵⁶ Briefly, 1,000 (or 500) simulated noisy data sets were generated by adding the standard deviation of the scatter about the least square fit, and the data sets were fitted with the model to generate 1,000 (or 500) sets of values for the model. These values were used to estimate the distributions of uncertainty of each parameter.

Results

Plasma glucose and glutamine

Blood plasma collected shortly after euthanasia did not vary significantly in total glucose concentrations when comparing [1-¹³C]glucose and [2-¹³C]glucose infused rats (12.7 ± 1.8 mM and 13.2 ± 1.2 mM, respectively, Student's t-test, p = 0.2; time course plasma glucose data available in supplementary information Figure S1), confirming that the concentration of glucose in the infused solutions and the infusion schemes used for the two sets of experiments were indeed identical. Likewise, glutamine concentrations in plasma were not significantly different (0.80 ± 0.09 mM and 0.79 ± 0.06 mM, respectively, Student's t-test, p = 0.6), confirming similar physiological conditions of the rats in the two sets of experiments.

The PE of plasma glucose-C1 and -C2 increased rapidly after the start of the respective infusions (52 ± 4% and 41 ± 2% at 8 min). PE remained stable throughout the time points measured, with the exception of a small but significant rise seen at 120 min for glucose-C1 (58 ± 3%, Student's t-test, p = 0.02) and at 60 and 120 min for glucose-C2 (46 ± 3% and 49 ± 1%; p < 0.01). Average PE from [1-¹³C]glucose infused rats was higher compared to rats receiving [2-¹³C]glucose (53 ± 4% and 44 ± 3% respectively, p < 0.0001). As explained with Figure S1, the difference may have arisen from inaccuracies in the percent enrichment of

Figure 2. Continued

diagonally striped circles: ¹³C-labeling is split between these positions; Red: Labeled position after first turn of the TCA cycle; Blue: Labeled position of the second turn of the TCA cycle; Green: Label position after entry of pyruvate carbons into the TCA cycle via pyruvate carboxylase (PC). The number '1' denotes the position of carbon number one in each molecule. All metabolic pathways are named in blue letters and illustrated by black arrows. Abbreviations: Glc: glucose; Pyr: pyruvate; AcCoA: Acetyl-Coenzyme A; αKG: α-ketoglutarate; OAA: oxaloacetate; Fum: fumarate; Asp: aspartate; Glu: glutamate; Gln: glutamine; GABA: gamma-aminobutyric acid; Vpdh: rate of pyruvate dehydrogenase; Vdil: rate of dilution; Vtca: rate of tricarboxylic acid cycle; Vefflux: rate of loss of carbon from the astrocytic TCA cycle via efflux of Gln from the brain, partly balanced by entry of glutamine from the blood at the rate Vdil_{Gln} (not shown); Vcyc_{GluGln}: rate of Glu/Gln-cycle; Vcyc_{GABAGln}: rate of GABA/Gln-cycle; Vpc: rate of pyruvate carboxylase; Vgad: rate of glutamate decarboxylase, GABA synthesis, Vgln: rate of glutamine synthesis; Vshunt: rate of the GABA shunt, i.e. GABA degradation in the GABAergic neuron; Vx: rate of aminotransferase. Designations 'GA', 'A' and 'N' after a pathway rate indicates rate in the GABAergic neuronal, astroglial and glutamatergic neuronal compartments, respectively.

the starting materials. The brain extract amino acid enrichments were normalized to the plasma glucose enrichments before they were introduced in the metabolic model, eliminating the effects of differences in glucose PE's on model output. More specifically, for each animal, the percentage ^{13}C -enrichment values of each brain metabolite carbon position was divided by the percentage ^{13}C -enrichment at plasma glucose C1 or C2, as appropriate and multiplied by 100. Minor glucose-C1 enrichment was observed in plasma of $[2-^{13}\text{C}]$ glucose infused animals, hence, the plasma $[1-^{13}\text{C}]$ glucose enrichments were also normalized to plasma glucose-C2 enrichment and included in the metabolic model. Raw data are provided in supplementary information as a Microsoft Excel file.

Assessment of source of glutamate and glutamine-C4 labeling in $[2-^{13}\text{C}]$ glucose-infused rat brain

Labeling above natural abundance was found in brain regions of rats infused with $[2-^{13}\text{C}]$ glucose, e.g. in CX following 120 min infusion, labeling reached an average of 3.4% at Glu-C4, 2.9% at Gln-C4 and 2.7% at GABA-C2 (Figure 3). As described previously,³⁶ labeling of these carbon positions may come from the pentose phosphate pathway or pyruvate recycling through malic enzyme (ME) in brain, or scrambling of the glucose label by the liver. Enrichment of glucose-C1 was detected in the respective plasma samples (3.6 ± 1.9 to $5.0 \pm 0.7\%$ during the 8-120 min infusions; Figure S1), indicating significant scrambling of the label in glucose by the liver, which we included in the modeling as an additional driver. Considering the combined dilutional fluxes given in supplementary information Table S4 into neuronal Glu at the level of Pyr or acetyl-CoA ($V_{\text{dil}_N}/V_{\text{tca}_N}$, 10%) and Gln ($V_{\text{dil}_{\text{Gln}}}/V_{\text{tca}_N}$, 19%), the CX glucose-C1 enrichment (and assuming equivalent label at C6) could provide 3–4% of the labeling at Glu-C4 observed in rats infused with $[2-^{13}\text{C}]$ glucose. This result was independent of the number of compartments comprising the model (compare Table S4 with Table S5, and see Figure S6-9 in supplementary information). Although the pentose phosphate pathway flux was not determined, its contribution to overall glucose metabolism is thought to be small ($\sim 1-5\%$).^{36,57,58} Thus, the labeling of Glu-C4 and its products following infusion with $[2-^{13}\text{C}]$ glucose can be explained totally by the combination of plasma glucose-C1 enrichment, the dilution and activity of the pentose phosphate cycle.

Brain tissue metabolite ^{13}C -labeling and metabolic rates

As expected, brain region extracts from rats infused with $[1-^{13}\text{C}]$ glucose or $[2-^{13}\text{C}]$ glucose showed a time

dependent increase in PE at all carbon positions measured, i.e. Glu-C2,C3,C4, Gln-C3,C4, and GABA-C2, C3,C4, and Asp-C2,C3. By 120 min of infusion with $[1-^{13}\text{C}]$ glucose, labeling at Glu-C4, Gln-C4 and GABA-C2 reached 30–40% (Figure 3), and formed the primary basis for estimating principal metabolic rates such as the rate of PDH, the TCA cycle and neurotransmitter cycling. In contrast to the labeling pattern seen with $[1-^{13}\text{C}]$ glucose, brain extracts from rats infused with $[2-^{13}\text{C}]$ glucose revealed that by 120 min of infusion, PE at Gln-C3, Glu-C3 and GABA-C3, which result predominantly from PC activity, reached 6–8%, clearly demonstrating that flux through this pathway is a smaller fraction of total glucose metabolism (Figure 3). Raw data are provided in supplementary information as a Microsoft Excel file.

The least-squares fitting of the three-compartment metabolic model to the labeling data from the $[1-^{13}\text{C}]$ and $[2-^{13}\text{C}]$ glucose infusions yielded estimates of V_{pc} and other fluxes. Examples of the best fits of the model for Glu-C2, C3, and C4, Gln-C3 and C4, GABA-C2, C3, and C4 and Asp-C2 and C3 time course data obtained for CX following $[1-^{13}\text{C}]$ and/or $[2-^{13}\text{C}]$ glucose infusions appear in Figure 3 (for the three other brain regions see supplementary information Figure S2, Figure S3 and Figure S4). Highly enriched carbon positions of large pool metabolites (e.g. Glu-C4 during infusions with $[1-^{13}\text{C}]$ glucose) exhibited relatively smaller scatter (%SD) compared to smaller pools with less labeling (e.g. GABA-C4 during $[2-^{13}\text{C}]$ glucose infusions), and thus were fitted with greater certainty by the metabolic model. The absolute scatter in terms of mM ^{13}C had the same magnitude for all metabolites measured (data not shown).

The metabolic rates derived by modeling of data from the four brain regions are summarized in Figure 4. Additional rates appear in Table S4 of supplementary information and Table S1 presents the mathematical relationships for the model.

V_{pc} varied approximately 44% across the four brain regions investigated, being lowest in CB and highest in ST, with intermediate values in CX and HP. Relative to total oxidative glucose consumption of neurons and astroglia ($\text{CMR}_{\text{glc(ox)}}$), V_{pc} constituted 13-19% and was lowest in CX and CB ($\sim 13\%$), intermediate in ST (16%), and highest in HP (19%). These results were independent of the number of model compartments (three versus two), producing the same regional pattern of absolute and relative V_{pc} values (Table 1), while differing by -2 to 7% (V_{pc}) and -4 to 10% ($V_{\text{pc}}/\text{CMR}_{\text{glc(ox)}}$), respectively (Table S4 versus Table S5). In contrast to the negligible effect on V_{pc} , V_{gln} and V_{cyc} , both astroglial and neuronal TCA cycle fluxes were increased for most brain regions by the addition of the third (GABAergic) compartment to

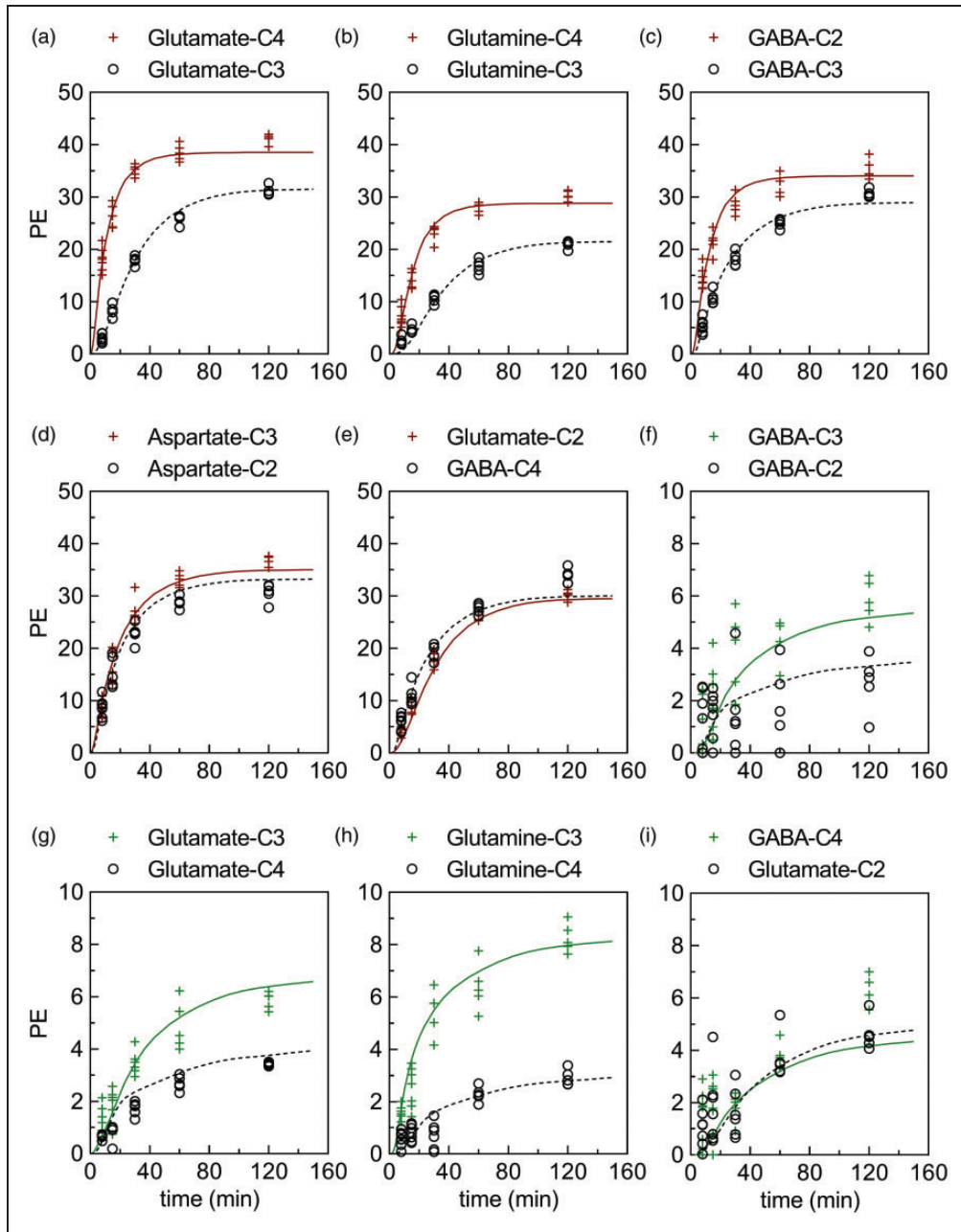


Figure 3. Best fits of the metabolic model (full red/green or dotted black lines) to experimental time course data from cerebral cortex (red/green plus and black circle symbols, respectively). The time courses for percentage ^{13}C -enrichment (PE) of (a–e) glutamate-C4,C3,C2, glutamine-C4,C3, GABA-C2,C3,C4, and aspartate-C2,C3 from $[1-^{13}\text{C}]$ glucose or (f–i) glutamate-C4,C3,C2, glutamine-C4,C3, and GABA-C2,C3,C4 from $[2-^{13}\text{C}]$ glucose infused rats obtained with ^1H - ^{13}C NMR. The time courses representing the cerebellum, hippocampus and striatum can be found in supplementary information Figure S2, Figure S3 and Figure S4, respectively. The majority (84 of 90) of time course data sets from cerebral cortex ($n = 5\text{--}7$ for each time point) passed the Shapiro-Wilk test for normality.

the model, with exception of V_{tca_A} for CB, which was reduced (Table 1).

When the CX data from the current study are grouped with literature values from studies of whole brain or cerebral cortex of anesthetized and awake

rats, a positive linear correlation was seen between V_{pc} and both $V_{\text{cyc}_{\text{Tot}}}$ (Figure 5(a)) and $\text{CMR}_{\text{glc(ox)}}$ (Figure 5(b)). In both cases, the corresponding fluxes for CB, HP and ST fell within the very broad confidence intervals of the best-fit lines, respectively.

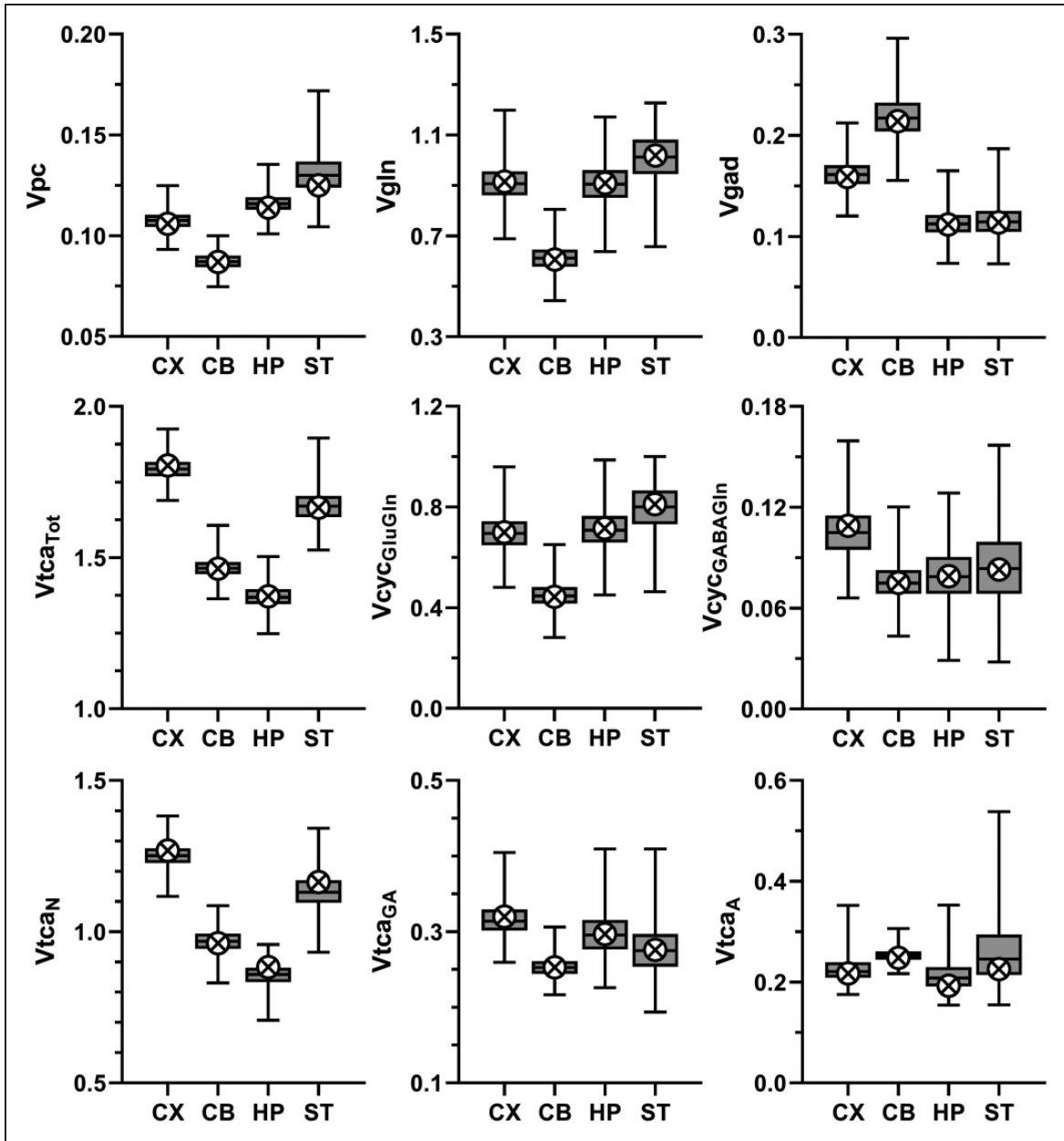


Figure 4. Selected metabolic rates ($\mu\text{mol/g/min}$) for cerebral cortex (CX), cerebellum (CB), hippocampus (HP) and striatum (ST) reported as best estimate (crossed circles) obtained from fitting of data to the three-compartment model and box-and-whiskers reporting minimum, 25th percentile, median, 75th percentile, and maximum for the frequency distribution determined from the Monte-Carlo analysis (MC). *Definitions:* V_{pc} , rate of anaplerosis via pyruvate carboxylase; V_{gln} , rate of glutamine synthesis via glutamine synthetase; V_{gad} , rate of GABA synthesis via glutamate decarboxylase (GAD); $V_{tca_{Tot}}$ ($=V_{tca_N} + V_{tca_A} + V_{tca_{GA}}$), rate of total TCA cycle; V_{tca_N} , $V_{tca_{GA}}$ and V_{tca_A} rate of TCA cycling in glutamatergic and GABAergic neurons, and astroglia, respectively; $V_{cyc_{GluGln}}$, rate of glutamate-glutamine cycling; $V_{cyc_{GABAGln}}$, rate of GABA-glutamine cycling. $V_{cyc_{GluGln}}$, $V_{cyc_{GABAGln}}$ and V_{tca_N} were iterated, whereas the other rates shown were calculated as specified in the model equations given in supplementary information Table S1. In supplementary information, additional rates appear in Table S4 and the frequency distribution for V_{pc} for all four brain regions are shown in Figure S5.

Moreover, linear regression analysis that included the CX data along with literature values from studies of rats over a large range of neural activities revealed the strong linear correlation previously reported between

the rates of total neuronal TCA cycling ($V_{tca_{N+GA}}$) and total neurotransmitter cycling ($V_{cyc_{Tot}}$) (Figure 5 (c)). Notably, the CX and other regions fell near the trend line in the plot of $V_{tca_{Tot}}$ versus $V_{cyc_{Tot}}$,

Table 1. Differences in best fit solutions of the three-compartment metabolic model compared to a two-compartment model for the selected fluxes.

Flux	Cerebral			
	cortex Δ (%)	Cerebellum Δ (%)	Hippocampus Δ (%)	Striatum Δ (%)
V _{cyc} *	-0.01	15.6	-5.2	3.7
V _{tca_N} *	12.9	21.2	13.4	14.4
V _{tca_A}	21.2	-17.6	80.4	21.0
V _{tca_{Tot}}	13.9	12.3	19.5	15.2
CMR _{glc(ox)}	8.6	7.4	11.0	8.6
V _{gln}	-0.8	13.3	-3.9	3.8
V _{pc}	-1.8	1.2	6.5	3.3

Values reflect the percentage difference in the best-fit solution to the three-compartment (3C) model versus a two-compartment (2C) model, i.e., $(3C/2C) \times 100$, for the given parameter. The asterisk (*) reflects the total flux for that parameter as specified by the model, e.g., for the three-compartment model $V_{cyc}^* = V_{cyc_{GluGln}} + V_{cyc_{GABAGln}}$ and $V_{tcaN}^* = V_{tcaN} + V_{tcaGA}$, reflecting the sums of the two neuronal (glutamatergic and GABAergic) compartments, whereas the two-compartment model represents these fluxes by single parameters, $V_{cyc_{GluGln}}$ and V_{tcaN} . The absolute values for these and other parameters are presented in Tables S4 and S5 of supplementary information.

although the CI is unreliable at high flux values due to paucity of available data for rats under awake conditions. Further details for this meta-analysis including statistical results are provided in Figure 5 and its legend.

Model validation

Besides the comparison with a two-compartment model described above, several other analysis were completed to validate the model. Results from these are provided, described and discussed in supplementary information. In particular, the local sensitivity of the metabolic model to certain parameters, which are either unknown or poorly determined and constrained as fixed values in the model, were tested one at a time for each of the four brain regions (Figure S10). These tests were supported by within-region correlation analyses of the Monte-Carlo evaluations across 35 of the rates (Figure S11). Furthermore, a detailed literature assessment was performed to justify the conclusion that the acute period of mild hypoglycemia of 8 min to 2 hours is not expected to affect the measured metabolic rates. Finally, the robustness of V_{pc} and certain other fluxes to the way in which astroglial glutamine dilution arose in the model was evaluated (Table S7).

Discussion

Anaplerosis is the primary metabolic pathway to replenish TCA cycle intermediates and neurotransmitter amino acids lost by diffusion or oxidation.¹⁻⁴ In the

brain, anaplerosis occurs predominately in astroglia and mainly through the ATP-dependent carboxylation of pyruvate by PC.⁵⁻¹⁰ While the evidence for the role of anaplerosis in ammonia detoxification is considerable,³ the extent to which glutamate/GABA oxidation and other potential mechanisms contribute to the PC flux *in vivo* remain open and debated questions. Regardless of the detailed mechanisms contributing to anaplerosis, the maintenance of constant levels of neurotransmitter amino acids and TCA cycle intermediates requires that this flux, as given by V_{pc} , balances all losses due to oxidation and diffusion. Thus, V_{pc} can be viewed as an upper bound of the net rate of glutamate/GABA oxidation, a process which involves malic enzyme, producing NADPH for reductive synthesis in anabolic processes,⁵⁹ reactive oxygen species scavenging^{60,61} and as a substrate for ROS-producing NADPH oxidases in signal transduction.⁶²

Previous measurements of PC flux in brain have focused on whole brain or a single brain region (e.g., cerebral cortex) and mostly in rodents under anesthesia. In this study, we used a sensitive NMR approach employing [2-¹³C]glucose, which provides a PC-specific labeling of metabolites,^{33,36} along with separate [1-¹³C] glucose infusions, which predominantly provides information on neuronal metabolism. We used these tools to obtain a detailed assessment of metabolism in multiple brain regions of awake rats, i.e. CB, HP, ST and CX. In a novel implementation of the three-compartment metabolic model, the two data sets were fitted simultaneously, yielding quantitative estimates of astroglial and neuronal metabolic rates in the measured brain regions. We also compared the flux estimates to those derived by a simpler two-compartment model composed of neurons (glutamatergic) and astroglia, and evaluated different astroglial dilution pathways to assess the robustness of our findings and their interpretation.

The rate of anaplerosis varies across brain regions of the awake rat

The value of V_{pc} for CX of 0.106 $\mu\text{mol}/\text{min}/\text{g}$, which constituted 13% of CMR_{glc(ox)}, is slightly lower than previously reported for whole brain in awake rats (0.14–0.18 $\mu\text{mol}/\text{min}/\text{g}$)³⁰ but larger than for CX and whole brain of rats under anesthesia (0.04–0.09 $\mu\text{mol}/\text{min}$ ^{19,20,25,26,63}). The variation across brain regions in CMR_{glc(ox)} follows the same order as reported for glucose consumption measured by Sokoloff et al.⁶⁴ using [¹⁴C]deoxyglucose, i.e. HP < CB < ST < CX. The relational order in the magnitudes of V_{pc} and CMR_{glc(ox)} among the different regions was not affected by the number of model compartments (three verses two: compare Table S4 and S5).

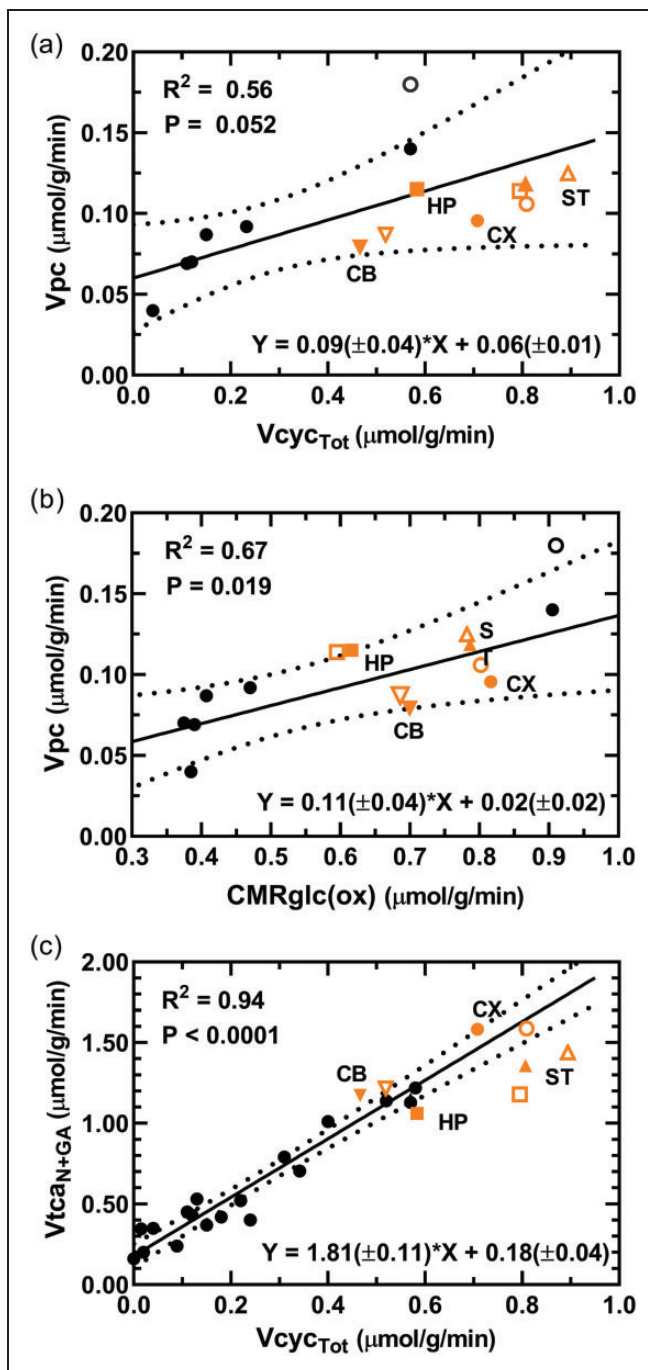


Figure 5. (a, b) Relationship between the rates of pyruvate carboxylation (V_{pc}) and total glutamate/GABA-glutamine cycling ($V_{cyc_{Tot}}$) and total glucose oxidation in neurons and astroglia ($CMR_{glc(ox)}$). The regression analyses include cerebral cortex data from the current study (CX; orange filled circle) and literature values from studies of whole brain or cerebral cortex (black circles;^{19,20,30,50,51,84,85}) of rats under awake and anesthetized conditions and where astroglial OAA-to-fumarate recycling was not allowed in the model, i.e., $V_{sc} = 0$ in the current study. Values for cerebellum (CB; inverted triangles), hippocampus (HP; squares) and striatum (ST; triangles) were superimposed on graphs for comparison but were not included in the regression analyses and parameters shown on the respective graphs. The unfilled symbols represent best-fit solutions allowing astroglial OAA-to-fumarate cycling for the corresponding brain region, which included the study by Öz et al (2004).³⁰ All brain regions fell within the 95% confidence interval of the best fit line. In a, including all brain regions in the least-squares best fit to the data yielded a line with slope of $0.08(\pm 0.02)$ and y-intercept of $0.06(\pm 0.01)$, $R^2 = 0.60$ and $P = 0.009$ (slope significantly different from zero). In b, including all brain regions in the least-squares best fit to the data yielded a line with slope of $0.11(\pm 0.03)$ and y-intercept of $0.03(\pm 0.02)$, $R^2 = 0.60$ and

Continued.

The value of V_{pc} varied by approximately 44% across the measured brain regions, being lowest in CB ($0.087 \pm 0.004 \mu\text{mol/g/min}$) and highest in ST (0.125 ± 0.009) with intermediate values in CX (0.106 ± 0.005) and HP (0.114 ± 0.005). The range of V_{pc} values determined for the four brain regions in the current study ($0.087\text{--}0.125 \mu\text{mol/g/min}$) is lower than what has been reported for the whole brain of awake rats, $0.17\text{--}0.18 \mu\text{mol/g/min}$.^{27,30} The lower value may reflect the methodology used with the two other studies using either $^{14}\text{CO}_2$ or $[1\text{-}^{13}\text{C}]\text{glucose}$ as the label precursor as discussed previously.³³

The value of V_{pc} in CX showed linear relationships with rates of glucose oxidation ($R^2 = 0.67$) and glutamate/glutamine cycling ($R^2 = 0.56$) when plotted against literature values reported for a large range of metabolic activity (Figure 5(a) and (b)), consistent with the activity dependent relationship noted previously.^{19,30,36,65,66} Moreover, data from CB, HP and ST fell within the 95% CI's of the cortical values. Neural activity as measured by electroencephalography (EEG) is correlated with $\text{CMR}_{\text{glc(ox)}}$ in human visual cortex.⁶⁷ Likewise, the relationship between changes in V_{cycTot} and $\text{CMR}_{\text{glcN(ox)}}$ for rat cortex is well established and suggests a close to 1:1 relationship⁶³ (or 1:2 for V_{cycTot} versus $V_{\text{tca}_{\text{N+GA}}}$). Plotting the values of V_{cycTot} against $V_{\text{tca}_{\text{N+GA}}}$ for the different regions shows that CX and CB fall near the best-fit line (and the 1:2 prediction) from the plot of the literature data, whereas HP and ST fell below this line (Figure 5(c)). This outcome was not affected by the number of model compartments (3 versus 2; compare Table S4 and S5). The lower $V_{\text{tca}_{\text{N+GA}}}/V_{\text{cycTot}}$ ratio for HP and ST is unclear, although for ST a similar conclusion was reached previously.⁶⁸ In this case, there are too few points at the high end of the scatter plot to calculate an appropriate 95% CI. Lower energy consumption for processes not involved in signaling in these regions might explain the lower ratios, although such information is not presently available. There may also be differences in the activity dependence of V_{pc} , which is subtracted from the value of V_{gln} in order to

calculate V_{cycTot} (recalling the model equation $V_{\text{gln}} = V_{\text{cyc}_{\text{GluGln}}} + V_{\text{cyc}_{\text{GABAGln}}} + V_{pc}$ and that $V_{\text{cycTot}} = V_{\text{cyc}_{\text{GABAGln}}} + V_{\text{cyc}_{\text{GluGln}}}$; see Table S1). Future studies of the different brain regions performed at different levels of neural activity using the same ^{13}C labeling methodology and animal model will be needed to resolve these issues.

Considering the relationship seen between V_{pc} and V_{cycTot} in cerebral cortex is linear and that the *regional* data points also align in a linear manner in Figure 5(a), suggests that a component of PC activity is coupled at a near constant ratio to *de novo* synthesis of glutamate needed to sustain neurotransmitter cycling, rather than ammonia detoxification and replacement of TCA cycle intermediates lost for purposes other than GABA/glutamate oxidation. V_{pc} constituted 12-14% of glutamine synthesis (V_{gln}) across brain regions, despite the 68% difference in rates of glutamine synthesis (being lowest in CB, $0.606 \pm 0.052 \mu\text{mol/g/min}$, and highest in ST, $1.019 \pm 0.100 \mu\text{mol/g/min}$). Anaplerosis thus appears to contribute equally to glutamine synthesis across brain regions of the awake rat. This further supports the proposed functional relationship between V_{cycTot} and V_{pc} .

Mechanisms contributing to anaplerotic flux

As noted above, anaplerosis balances the combined losses of neurotransmitter amino acids and precursor substrates through ammonia detoxification, diffusion and oxidation. Under normal physiological conditions and low blood ammonia level, oxidation is thought to be the dominate route of glutamate and GABA loss, and thus, this rate is maximally bounded by V_{pc} .^{44,59} An estimate of the non-signaling (housekeeping) component of V_{pc} that includes ammonia detoxification for cerebral cortex is given by the y-axis intercept ($V_{\text{cyc}} = 0$) of the least-squares fitted line in the plot of V_{pc} versus V_{cycTot} (Figure 5(a)) of $0.06 \mu\text{mol/g/min}$. This value is higher than values of brain glutamine efflux measured in anesthetized rats of ~ 0 to $0.02 \mu\text{mol/min/g}$ ⁶⁹⁻⁷¹ using ^{13}N and ^{15}N labeled ammonia and arterio-venous difference methods (for a

Figure 5. Continued

$P = 0.008$ (slope significantly different from zero). (c) Relationship between the total TCA cycling in neurons ($V_{\text{tca}_{\text{N+GA}}} = V_{\text{tca}_{\text{N}}} + V_{\text{tca}_{\text{GA}}}$) and total glutamate and GABA neurotransmitter cycling ($V_{\text{cycTot}} = V_{\text{cyc}_{\text{GluGln}}} + V_{\text{cyc}_{\text{GABAGln}}}$). The regression analysis includes CX data from the current study (orange circle) and literature values from studies of anesthetized and awake rats (black circles; e.g. awake or using α -chloralose, morphine, halothane, different doses of pentobarbital, or urethane;^{19,20,25,26,30,49,50,84-87}). Values for CB, HP and ST data from the current study are superimposed for comparison but were not included for the regression analysis and the parameters shown on the respective graphs. In c, including all brain regions in the least-squares best fit to the data yielded a line with slope of $1.68(\pm 0.10)$ and y-intercept of $0.20(\pm 0.04)$, $R^2 = 0.93$ and $P < 0.0001$ (slope significantly different from zero). (a-c) All literature values included in the analyses derive from studies performed on rats using ^{13}C -labeled substrates and *in vivo* or *ex vivo* NMR. On all graphs a trend line and 95% confidence intervals are shown along with the parameters from the regression analysis: R^2 , Pearson product-moment correlation coefficient; P value, significance of the difference in the value of the slope from zero; equation with slope and y-intercept, \pm SE.

summary see³³) suggesting that much of the PC flux measured in awake animals under physiologically normal conditions is not driven by ammonia fixation and removal.

Whereas glutamate and GABA oxidation is readily measured in brain slices^{72–75} and cultured astroglia (and to some degree in cultured neurons and isolated synaptosomes),^{2,76–78} direct demonstration of their oxidation *in vivo*, as evidenced by ¹³C labeling patterns consistent with astrocyte pyruvate recycling, has not been found. In astroglia, the magnitude of glutamate oxidation is strongly determined by the extracellular glutamate concentration, rising significantly for levels >100 μM^2 , which is \sim 100-fold higher than the ambient extracellular level measured by microdialysis *in vivo*.^{79,80} Complete oxidation of glutamate and GABA in the TCA cycle can be achieved *via* mitochondrial ME, which decarboxylates malate to pyruvate followed by its conversion to acetyl-CoA by PDH and oxidation in the TCA cycle. Pyruvate recycling through ME-PDH produces distinct labeling patterns in glutamate and glutamine depending on the labeled carbon position in glucose. For example, the subsequent action of ME on the ¹³C-labeled OAA-C2 and C3 (after recycling to malate-C2 and C3 *via* back flow to fumarate) produced from [2-¹³C]glucose-derived pyruvate-C2 *via* PC would produce both C2- and C3-labeled pyruvate, leading to Glu-C4 (and Gln-C4) labeling from [2-¹³C]glucose, which was observed in the present study. In addition to pyruvate recycling through ME-PDH, an alternate pathway that shunts the flow from malate to OAA through pyruvate (bypassing MDH) by coupling ME with PC has been described.⁸¹ In pyruvate recycling through ME-PC, one molecule of NADPH is produced and one molecule of ATP hydrolyzed for each molecule of malate converted to OAA. Unfortunately, flux through ME-PDH and ME-PC will produce the same ¹³C labeling patterns from [2-¹³C]glucose, and thus cannot be differentiated in this manner. In addition, due to label scrambling between malate C3 and C2 (back flow through fumarate to fumarate; denoted by Vsc in the model), pyruvate recycling through ME-PC will tend to equalize labeling between pyruvate-C2 and C3, and thus also between OAA-C3 and C2 *via* PC (and glutamine C3 and C2). The large difference in ¹³C enrichment between glutamine C3 and C2 suggests that pyruvate recycling through ME-PC is not the major component of PC flux.

As noted above, Glu-C4 and Gln-C4 labeling from [2-¹³C]glucose was observed, consistent with pyruvate recycling. However, other pathways are known to contribute to this labeling, namely label scrambling in blood glucose by hepatic metabolism and the pentose phosphate pathway (PPP). In the present study,

scrambling of the label in plasma glucose from C2 to C1 could explain approximately half of the \sim 3% enrichment seen in Glu-C4, Gln-C4 and GABA-C2. In a previous study of anesthetized rats,³⁶ labeling in Glu-C4 after infusion of [2-¹³C]glucose was compared with that from [5-¹³C]glucose, which is not confounded by metabolism through the PPP, finding that \sim 1% of the Glu-C4 labeling was derived from this pathway. As pointed out previously,⁸² the anticipated fractional enrichment of ¹³C labeling due to pyruvate recycling in astroglia is low and may be below the ability to differentiate from blood contributions. Thus, our findings support previous *in vivo* and *ex vivo* studies where brain and blood enrichments were determined^{20,36,83} in finding no definitive evidence for pyruvate recycling (whether by ME-PDH or ME-PC), leaving unanswered questions about the quantitative significance of glutamate oxidation⁵⁹ and (or) NADPH production and ROS scavenging⁸¹ in anaplerosis and the crucial need for further investigation.

Conclusions

Simultaneous fitting to a three-compartment metabolic model of 18 enrichment (%) time courses from metabolism of [1-¹³C] and [2-¹³C]glucose in four brain regions and blood plasma was successfully performed and 35 metabolic fluxes determined. The pyruvate carboxylase flux (Vpc) across the four brain regions of the awake rat varied from 0.087 to 0.125 $\mu\text{mol}/\text{min}/\text{g}$ in the order CB<CX<HP<ST.

Vpc constituted 6-8% of total TCA cycle flux and accounted for 12-14% of glutamine synthesis. Furthermore, Vpc varied linearly with the rates of neurotransmitter cycling and total glucose oxidation, with the four brain regions mapping well within the 95% confidence interval. This suggests a functional role of Vpc, supporting different signaling and energetic demands of the different brain regions.

Funding

The author(s) disclosed receipt of the following financial support for the research, authorship, and/or publication of this article: LMM acknowledges the Department of Drug Design and Pharmacology (UCPH, Denmark) for granting of a PhD scholarship. This work was supported in part by NIH NIMH grants MH095104 and MH109159, NIH NIDDK grant R01 DK108283, NIH NIAAA grant R01 AA021984 and R21 AA028628, and a grant from Aase og Ejnar Danielsens Fond.

Acknowledgements

We thank Ms. Monique Thomas for her helpful guidance with regards to tissue extractions, Dr. Robin de Graaf for providing the ¹H-[¹³C]-NMR sequence and Terry Nixon, Scott McIntyre and Peter Brown for engineering and

maintenance support of the NMR spectrometer. Jens V Andersen is acknowledged for helpful assistance with the manuscript.


Declaration of conflicting interests

The author(s) declared no potential conflicts of interest with respect to the research, authorship, and/or publication of this article.

Authors' contributions

LMM, KB, GFM, DLR and HSW conceptualized and designed the study. LMM conducted all experiments with support from XM, GMIC and LJ (live animal procedures, sample processing), LJ, KB and GFM (NMR acquisition, data processing and modeling of data). LMM drafted the manuscript in collaboration with HSW, KB, GFM and DLR. All co-authors revised the manuscript and approved the version to be published.

ORCID iD

Laura M McNair  <https://orcid.org/0000-0002-5213-9931>

Supplemental material

Supplemental material for this article is available online.

References

- Sonnevald U, Westergaard N, Jones P, et al. Metabolism of [U-¹³C₅] glutamine in cultured astrocytes studied by NMR spectroscopy: first evidence of astrocytic pyruvate recycling. *J Neurochem* 1996; 67: 2566–2572.
- McKenna MC, Sonnevald U, Huang X, et al. Exogenous glutamate concentration regulates the metabolic fate of glutamate in astrocytes. *J Neurochem* 1996; 66: 386–393.
- Cooper AJ and Plum F. Biochemistry and physiology of brain ammonia. *Physiol Rev* 1987; 67: 440–519.
- Cruz F, Scott SR, Barroso I, et al. Ontogeny and cellular localization of the pyruvate recycling system in rat brain. *J Neurochem* 1998; 70: 2613–2619.
- Patel MS. The effect of ketone bodies on pyruvate carboxylation by rat brain mitochondria. *J Neurochem* 1974; 23: 865–867.
- Carter CJ, Savasta M, Fage D, et al. 2-Oxo-[¹⁴C]glutarate is taken up by glutamatergic nerve terminals in the rat striatum. *Neurosci Lett* 1986; 72: 227–231.
- Cesar M and Hamprecht B. Immunocytochemical examination of neural rat and mouse primary cultures using monoclonal antibodies raised against pyruvate carboxylase. *J Neurochem* 1995; 64: 2312–2318.
- Shank RP, Bennett GS, Freytag SO, et al. Pyruvate carboxylase: an astrocyte-specific enzyme implicated in the replenishment of amino acid neurotransmitter pools. *Brain Res* 1985; 329: 364–367.
- Sonnevald U, Westergaard N, Hassel B, et al. NMR spectroscopic studies of ¹³C acetate and ¹³C glucose metabolism in neocortical astrocytes: evidence for mitochondrial heterogeneity. *Dev Neurosci* 1993; 15: 351–358.
- Yu AC, Drejer J, Hertz L, et al. Pyruvate carboxylase activity in primary cultures of astrocytes and neurons. *J Neurochem* 1983; 41: 1484–1487.
- Bradford HF, Ward HK and Thomas AJ. Glutamine – a major substrate for nerve endings. *J Neurochem* 1978; 30: 1453–1459.
- Laake JH, Slyngstad TA, Haug FM, et al. Glutamine from glial cells is essential for the maintenance of the nerve terminal pool of glutamate: immunogold evidence from hippocampal slice cultures. *J Neurochem* 1995; 65: 871–881.
- Paulsen RE, Odden E and Fonnum F. Importance of glutamine for gamma-aminobutyric acid synthesis in rat neostriatum in vivo. *J Neurochem* 1988; 51: 1294–1299.
- Peng L, Hertz L, Huang R, et al. Utilization of glutamine and of TCA cycle constituents as precursors for transmitter glutamate and GABA. *Dev Neurosci* 1993; 15: 367–377.
- Reubi JC, Van Der Berg C and Cuénod M. Glutamine as precursor for the GABA and glutamate transmitter pools. *Neurosci Lett* 1978; 10: 171–174.
- Rothstein JD and Tabakoff B. Alteration of striatal glutamate release after glutamine synthetase inhibition. *J Neurochem* 1984; 43: 1438–1446.
- Thanki CM, Sugden D, Thomas AJ, et al. In vivo release from cerebral cortex of [¹⁴C]glutamate synthesized from [U-¹⁴C]glutamine. *J Neurochem* 1983; 41: 611–617.
- Ward HK, Thanki CM and Bradford HF. Glutamine and glucose as precursors of transmitter amino acids: ex vivo studies. *J Neurochem* 1983; 40: 855–860.
- Choi IY, Lei H and Gruetter R. Effect of deep pentobarbital anesthesia on neurotransmitter metabolism in vivo: on the correlation of total glucose consumption with glutamatergic action. *J Cereb Blood Flow Metab* 2002; 22: 1343–1351.
- Duarte JM, Lanz B and Gruetter R. Compartmentalized cerebral metabolism of [1,6-¹³C]glucose determined by in vivo ¹³C NMR spectroscopy at 14.1 T. *Front Neuroenergetics* 2011; 3
- Griffin JL, Rae C, Radda GK, et al. Lactate-induced inhibition of glucose catabolism in guinea pig cortical brain slices. *Neurochem Int* 1999; 35: 405–409.
- Hassel B, Sonnevald U and Fonnum F. Glial-neuronal interactions as studied by cerebral metabolism of [2-¹³C] acetate and [1-¹³C]glucose: an ex vivo ¹³C NMR spectroscopic study. *J Neurochem* 2002; 64: 2773–2782.
- Kanamatsu T and Tsukada Y. Effects of ammonia on the anaplerotic pathway and amino acid metabolism in the brain: an ex vivo ¹³C NMR spectroscopic study of rats after administering [2-¹³C] glucose with or without ammonium acetate. *Brain Res* 1999; 841: 11–19.
- Melø TM, Nehlig A and Sonnevald U. Neuronal-glial interactions in rats fed a ketogenic diet. *Neurochem Int* 2006; 48: 498–507.

25. Patel AB, Chowdhury GM, de Graaf RA, et al. Cerebral pyruvate carboxylase flux is unaltered during bicuculline-seizures. *J Neurosci Res* 2005; 79: 128–138.
26. Patel AB, de Graaf RA, Mason GF, et al. Glutamatergic neurotransmission and neuronal glucose oxidation are coupled during intense neuronal activation. *J Cereb Blood Flow Metab* 2004; 24: 972–985.
27. Serres S, Raffard G, Franconi JM, et al. Close coupling between astrocytic and neuronal metabolisms to fulfill anaplerotic and energy needs in the rat brain. *J Cereb Blood Flow Metab* 2008; 28: 712–724.
28. Shank RP, Leo GC and Zielke HR. Cerebral metabolic compartmentation as revealed by nuclear magnetic resonance analysis of D-[1-¹³C]glucose metabolism. *J Neurochem* 1993; 61: 315–323.
29. Tiwari V and Patel AB. Pyruvate carboxylase and pentose phosphate fluxes are reduced in A β PP-PS1 mouse model of Alzheimer's disease: a ¹³C NMR study. *J Alzheimers Dis* 2014; 41: 387–399.
30. Öz G, Berkich DA, Henry PG, et al. Neuroglial metabolism in the awake rat brain: CO₂ fixation increases with brain activity. *J Neurosci* 2004; 24: 11273–11279.
31. Gruetter R, Seaquist ER, Kim S, et al. Localized in vivo ¹³C-NMR of glutamate metabolism in the human brain: initial results at 4 tesla. *Dev Neurosci* 1998; 20: 380–388.
32. Gruetter R, Seaquist ER and Ugurbil K. A mathematical model of compartmentalized neurotransmitter metabolism in the human brain. *Am J Physiol Endocrinol Metab* 2001; 281: E100–12.
33. Mason GF, Petersen KF, de Graaf RA, et al. Measurements of the anaplerotic rate in the human cerebral cortex using ¹³C magnetic resonance spectroscopy and [1-¹³C] and [2-¹³C] glucose. *J Neurochem* 2007; 100: 73–86.
34. Sonnay S, Poirot J, Just N, et al. Astrocytic and neuronal oxidative metabolism are coupled to the rate of glutamate-glutamine cycle in the tree shrew visual cortex. *Glia* 2018; 66: 477–491.
35. Sonnay S, Duarte JM, Just N, et al. Compartmentalised energy metabolism supporting glutamatergic neurotransmission in response to increased activity in the rat cerebral cortex: a ¹³C MRS study in vivo at 14.1 T. *J Cereb Blood Flow Metab* 2016; 36: 928–940.
36. Sibson NR, Mason GF, Shen J, et al. In vivo ¹³C NMR measurement of neurotransmitter glutamate cycling, anaplerosis and TCA cycle flux in rat brain during [2-¹³C] glucose infusion. *J Neurochem* 2001; 76: 975–989.
37. Taylor A, McLean M, Morris P, et al. Approaches to studies on neuronal/glia relationships by ¹³C-MRS analysis. *Dev Neurosci* 1996; 18: 434–442.
38. Berl S, Takagaki G, Clarke DD, et al. Carbon dioxide fixation in the brain. *J Biol Chem* 1962; 237: 2570–2573.
39. Rossi CA, Berl S, Clarke DD, et al. Rate of CO₂ fixation in brain and liver. *Life Sci (1962)* 1962; 1: 533–539.
40. Keech DB and Utter MF. Pyruvate carboxylase. *J Biol Chem* 1963; 238: 2609–2614.
41. Schousboe A, Waagepetersen HS and Sonnewald U. Astrocytic pyruvate carboxylation: status after 35 years. *J Neurosci Res* 2019; 97: 890–896.
42. McMillan PJ and Mortensen RA. The metabolism of brain pyruvate and acetate in the tricarboxylic acid cycle. *J Biol Chem* 1963; 238: 91–93.
43. O'Neal RM and Koeppe RE. Precursors in vivo of glutamate, aspartate and their derivatives of rat brain. *J Neurochem* 1966; 13: 835–847.
44. Hertz L and Rothman DL. Glutamine-glutamate cycle flux is similar in cultured astrocytes and brain and both glutamate production and oxidation are mainly catalyzed by aspartate aminotransferase. *Biology (Basel)* 2017; 6: 17.
45. Fitzpatrick SM, Hetherington HP and Behar KL. The flux from glucose to glutamate in the rat brain in vivo as determined by ¹H-observed, ¹³C-edited NMR spectroscopy. *J Cereb Blood Flow Metab* 1990; 10: 170–179.
46. de Graaf RA, Chowdhury GM, Brown PB, et al. In situ 3D magnetic resonance metabolic imaging of microwave-irradiated rodent brain: a new tool for metabolomics research. *J Neurochem* 2009; 109: 494–501.
47. de Graaf RA, Mason GF, Patel AB, et al. In vivo ¹H-[¹³C]-NMR spectroscopy of cerebral metabolism. *NMR Biomed* 2003; 16: 339–357.
48. Chowdhury GM, Gupta M, Gibson KM, et al. Altered cerebral glucose and acetate metabolism in succinic semialdehyde dehydrogenase-deficient mice: evidence for glial dysfunction and reduced glutamate/glutamine cycling. *J Neurochem* 2007; 103: 2077–2091.
49. Chowdhury GM, Patel AB, Mason GF, et al. Glutamatergic and GABAergic neurotransmitter cycling and energy metabolism in rat cerebral cortex during postnatal development. *J Cereb Blood Flow Metab* 2007; 27: 1895–1907.
50. Duarte JM and Gruetter R. Glutamatergic and GABAergic energy metabolism measured in the rat brain by ¹³C NMR spectroscopy at 14.1 T. *J Neurochem* 2013; 126: 579–590.
51. Patel AB, de Graaf RA, Mason GF, et al. The contribution of GABA to glutamate/glutamine cycling and energy metabolism in the rat cortex in vivo. *Proc Natl Acad Sci U S A* 2005; 102: 5588–5593.
52. Mason GF, Martin DL, Martin SB, et al. Decrease in GABA synthesis rate in rat cortex following GABA-transaminase inhibition correlates with the decrease in GAD₆₇ protein. *Brain Res* 2001; 914: 81–91.
53. Mason GF, Falk Petersen K, de Graaf RA, et al. A comparison of ¹³C NMR measurements of the rates of glutamine synthesis and the tricarboxylic acid cycle during oral and intravenous administration of [1-¹³C]glucose. *Brain Res Brain Res Protoc* 2003; 10: 181–190.
54. Mason GF. CWave: software for the design and analysis of ¹³C-labeling studies performed in vivo. *Proc Intl Soc Mag Reson Med* 2000; 8: 1870.
55. Kuwabara H, Evans AC and Gjedde A. Michaelis-Menten constraints improved cerebral glucose

- metabolism and regional lumped constant measurements with [^{18}F]fluorodeoxyglucose. *J Cereb Blood Flow Metab* 1990; 10: 180–189.
56. Mason GF, Rothman DL, Behar KL, et al. NMR determination of the TCA cycle rate and alpha-ketoglutarate/glutamate exchange rate in rat brain. *J Cereb Blood Flow Metab* 1992; 12: 434–447.
57. Ben-Yoseph O, Boxer PA and Ross BD. Noninvasive assessment of the relative roles of cerebral antioxidant enzymes by quantitation of pentose phosphate pathway activity. *Neurochem Res* 1996; 21: 1005–1012.
58. Hostetler KY and Landau BR. Estimation of the pentose cycle contribution to glucose metabolism in tissue in vivo. *Biochemistry* 1967; 6: 2961–2964.
59. Sonnewald U. Glutamate synthesis has to be matched by its degradation – where do all the carbons go? *J Neurochem* 2014; 131: 399–406.
60. Hothersall JS, El-Hassan A, McLean P, et al. Age-related changes in enzymes of rat brain. 2. Redox systems linked to NADP and glutathione. *Enzyme* 1981; 26: 271–276.
61. Andrés A, Satrústegui J and Machado A. Development of NADPH-consuming pathways in heart, brain and liver of the rat. *Biol Neonate* 1983; 43: 198–204.
62. Fang J, Sheng R and Qin ZH. NADPH oxidases in the central nervous system: regional and cellular localization and the possible link to brain diseases. *Antioxid Redox Signal* 2021; 35: 951–973.
63. Hyder F, Patel AB, Gjedde A, et al. Neuronal-glial glucose oxidation and glutamatergic-GABAergic function. *J Cereb Blood Flow Metab* 2006; 26: 865–877.
64. Sokoloff L, Reivich M, Kennedy C, et al. The [^{14}C]deoxyglucose method for the measurement of local cerebral glucose utilization: theory, procedure, and normal values in the conscious and anesthetized albino rat. *J Neurochem* 1977; 28: 897–916.
65. Shen J, Sibson NR, Cline G, et al. ^{15}N -NMR spectroscopy studies of ammonia transport and glutamine synthesis in the hyperammonemic rat brain. *Dev Neurosci* 1998; 20: 434–443.
66. Öz G, Okar DA. and Henry PG Glutamate-glutamine cycle and anaplerosis. In: Choi IY and Gruetter R (eds). *Neural metabolism in vivo*. Vol. 4. Springer: Boston, MA, 2012. pp. 921–946.
67. Hyder F, Fulbright RK, Shulman RG, et al. Glutamatergic function in the resting awake human brain is supported by uniformly high oxidative energy. *J Cereb Blood Flow Metab* 2013; 33: 339–347.
68. Wang J, Jiang L, Jiang Y, et al. Regional metabolite levels and turnover in the awake rat brain under the influence of nicotine. *J Neurochem* 2010; 113: 1447–1458.
69. Hawkins RA, Miller AL, Nielsen RC, et al. The acute action of ammonia on rat brain metabolism in vivo. *Biochem J* 1973; 134: 1001–1008.
70. Gjedde A, Lockwood AH, Duffy TE, et al. Cerebral blood flow and metabolism in chronically hyperammonemic rats: effect of an acute ammonia challenge. *Ann Neurol* 1978; 3: 325–330.
71. Dejong CH, Deutz NE and Soeters PB. Cerebral cortex ammonia and glutamine metabolism in two rat models of chronic liver insufficiency-induced hyperammonemia: influence of pair-feeding. *J Neurochem* 1993; 60: 1047–1057.
72. Andersen JV, Nissen JD, Christensen SK, et al. Impaired hippocampal glutamate and glutamine metabolism in the db/db mouse model of type 2 diabetes mellitus. *Neural Plast* 2017; 2017: 2107084.
73. Voss CM, Andersen JV, Jakobsen E, et al. AMP-activated protein kinase (AMPK) regulates astrocyte oxidative metabolism by balancing TCA cycle dynamics. *Glia* 2020; 68: 1824–1839.
74. Balazs R, Machiyama Y, Hammond BJ, et al. The operation of the gamma-aminobutyrate bypath of the tricarboxylic acid cycle in brain tissue in vitro. *Biochem J* 1970; 116: 445–461.
75. Andersen JV, Jakobsen E, Westi EW, et al. Extensive astrocyte metabolism of γ -aminobutyric acid (GABA) sustains glutamine synthesis in the mammalian cerebral cortex. *Glia* 2020; 68: 2601–2612.
76. Yu AC, Schousboe A and Hertz L. Metabolic fate of ^{14}C -labeled glutamate in astrocytes in primary cultures. *J Neurochem* 1982; 39: 954–960.
77. Waagepetersen HS, Qu H, Hertz L, et al. Demonstration of pyruvate recycling in primary cultures of neocortical astrocytes but not in neurons. *Neurochem Res* 2002; 27: 1431–1437.
78. Andersen JV, Markussen KH, Jakobsen E, et al. Glutamate metabolism and recycling at the excitatory synapse in health and neurodegeneration. *Neuropharmacology* 2021; 196: 108719.
79. Baker DA, Xi ZX, Shen H, et al. The origin and neuronal function of in vivo nonsynaptic glutamate. *J Neurosci* 2002; 22: 9134–9141.
80. Lerma J, Herranz AS, Herreras O, et al. In vivo determination of extracellular concentration of amino acids in the rat hippocampus. A method based on brain dialysis and computerized analysis. *Brain Res* 1986; 384: 145–155.
81. DiNuzzo M, Giove F, Maraviglia B, et al. Computational flux balance analysis predicts that stimulation of energy metabolism in astrocytes and their metabolic interactions with neurons depend on uptake of K^+ rather than glutamate. *Neurochem Res* 2017; 42: 202–216.
82. Lebon V, Petersen KF, Cline GW, et al. Astroglial contribution to brain energy metabolism in humans revealed by ^{13}C nuclear magnetic resonance spectroscopy: elucidation of the dominant pathway for neurotransmitter glutamate repletion and measurement of astrocytic oxidative metabolism. *J Neurosci* 2002; 22: 1523–1531.
83. Serres S, Bezancon E, Franconi JM, et al. Brain pyruvate recycling and peripheral metabolism: an NMR analysis ex vivo of acetate and glucose metabolism in the rat. *J Neurochem* 2007; 101: 1428–1440.

84. Jeffrey FM, Marin-Valencia I, Good LB, et al. Modeling of brain metabolism and pyruvate compartmentation using ^{13}C NMR in vivo: caution required. *J Cereb Blood Flow Metab* 2013; 33: 1160–1167.
85. Lanz B, Xin L, Millet P, et al. In vivo quantification of neuro-glial metabolism and glial glutamate concentration using ^1H - ^{13}C MRS at 14.1T. *J Neurochem* 2014; 128: 125–139.
86. de Graaf RA, Mason GF, Patel AB, et al. Regional glucose metabolism and glutamatergic neurotransmission in rat brain in vivo. *Proc Natl Acad Sci U S A* 2004; 101: 12700–12705.
87. Sibson NR, Dhankhar A, Mason GF, et al. Stoichiometric coupling of brain glucose metabolism and glutamatergic neuronal activity. *Proc Natl Acad Sci U S A* 1998; 95: 316–321.